TESTING THE USE OF $^{210}Pb_{ex}$ TO STUDY SEDIMENT CONNECTIVITY IN A MEDITERRANEAN MOUNTAIN BASIN WITH BADLANDS

Mariano Moreno-de las Heras[1*], Francesc Gallart[1], Jérôme Latron[1], Núria Martínez-Carreras[2], Laura Ferrer[3] and Joan Estrany[4]

(1) Institute of Environmental Assessment and Water Research (IDAEA), Spanish Research Council (CSIC), Jordi Girona 18, 08034 Barcelona, Spain.

(2) Luxembourg Institute of Science and Technology (LIST), 41, Rue du Brill, 4422 Belvaux, Luxembourg.

(3) Environmental Radioactivity Laboratory (LaboRA), University of the Balearic Islands, Ctra. Valldemossa km 7.5, 07122 Palma de Mallorca, Spain.

(4) Department of Geography, University of the Balearic Islands, Ctra. Valldemossa km 7.5, 07122 Palma de Mallorca, Spain.

*Correspondence to: M. Moreno-de las Heras, Surface Hydrology and Erosion Group, IDAEA, CSIC, Jordi Girona 18, 08034 Barcelona, Spain. Phone: +34 93 4006100, fax: +34 93 2045904, e-mail: mariano.moreno@idaea.csic.es

ABSTRACT

Basin management demands a sound understanding of sediment dynamics, particularly in Mediterranean mountain catchments with badlands, which affect water bodies and freshwater ecosystems. Connectivity has emerged as a framework for understanding how sediments move between geomorphic zones. We analyse the feasibility of excess lead-210 ($^{210}Pb_{ex}$) to study sediment connectivity in a 4-km^2 Mediterranean mountain basin with badlands (Vallcebre research catchments, Eastern Pyrenees) by applying mass-balance models for hypothesis generation and experimental testing. Badlands in the area are weathered by freezing during the winter and are eroded in summer by high-intensity showers. The eroded sediments may remain deposited within the streams from months to years. Application of $^{210}Pb_{ex}$ balance models in our basin suggests: (i) a saw-tooth seasonal pattern of badland surface $^{210}Pb_{ex}$ activities (increasing from October to May, and depleted in summer) and (ii) a downstream increase in sediment activity due to fallout lead-210 accumulation in streambed sediment deposits. Our experimental results (obtained during 2013 and 2014) showed low sediment $^{210}Pb_{ex}$ concentrations, illustrating the fresh-rock origin of sediments, but also hampering their study due to high measurement uncertainty (especially for sediments with d50>20µm) and dependence on sampling methods. Suspended sediment $^{210}Pb_{ex}$ activity reproduced the simulated seasonal activity patterns for the badland surfaces. However, sediment activity decreased downstream, suggesting that flushing of fine sediments by flooding prevents fallout lead-210 accumulation on the streambed. Overall, high sediment connectivity was revealed between the badlands, streams and outlet of the basin, as well as the fast transmission of $^{210}Pb_{ex}$ by the finest sediment fraction.

KEY WORDS: sediment connectivity, excess lead-210, sediment sampling methods, suspended sediment transport, badlands, Mediterranean mountain catchments, Vallcebre research catchments.

INTRODUCTION

Soil erosion and fluvial sediment transport are physical processes that are recognized as significant environmental problems in many Mediterranean areas. In this region, the interaction between seasonally contrasted climate, rugged topography, variable lithology and a long history of human pressures have led to intense erosion and high sediment loads that may potentially affect the sedimentary structure of rivers, the river biota and the quality of water supplies for human uses (Wainwright & Thornes 2004; Gallart *et al*. 2013; Garcia-Ruiz *et al*. 2013). Recent explorations of sediment yield data collected in more than 5,000 reservoirs and 1,200 gauging stations in European river basins revealed that Mediterranean rivers transport higher amounts of sediments than rivers in other regions and suggested that reservoir siltation may be a matter of concern (Vanmaercke *et al*. 2011). It is well known, however, that most sediment load is generated by soil erosion *hotspots* in relatively small sections of the terrain (Nadal-Romero *et al*. 2011; López-Tarazón *et al*. 2012; Gallart *et al*. 2013; García-Ruiz *et al*. 2017). In Mediterranean mountain catchments, highly-erodible landforms representing, in general, minor catchment fractions, such as badlands, contribute much of the total sediment transported within the regional drainage network, therefore impacting channel and floodplain dynamics as well as freshwater ecosystems (Clotet 1984; Mano *et al*. 2009; Moreno-de las Heras & Gallart 2016). Thus, analysis of sediment dynamics in Mediterranean environments is fundamental to basin management, particularly for mountain catchments with badlands.

Small to mesoscale mountain catchments provide excellent landscape settings for the study of hydrological and sediment relationships between hillslopes, where the main runoff and sediment sources are located, and streams, where sediment transfer, deposition and channel scouring takes place (Gallart *et al*. 2002; Nadal-Romero *et al*. 2008; Latron *et al*. 2009; López-Tarazón *et al*. 2012). Extensive meta-analysis of the sediment budget for Mediterranean basins with badlands ranging from approx. 1 ha to over 500 km^2 indicated that sediment yield decreases with scale, owing to a reduction in the proportion of highly erosive landforms and the effect of sediment storage on geomorphological sinks, such as topographical concavities, debris fans and streambeds (Nadal-Romero *et al.* 2011). Sediment transfer in Mediterranean mountain basins not only varies in space, but also in time (Duvert *et al*. 2012). Temporal aspects are mainly related to the size and frequency of sediment transfer processes. In fact, the temporal dynamics of rainfall intensity and flood magnitude greatly affect the distribution and activity of sources, stores and sinks of sediments, which ultimately reflect the routes, travel distances and pathways of sediment transfer (Bracken & Croke 2007; Nadal-Romero *et al*. 2008; Gallart *et al*. 2013).

Sediment budget analysis by standard sediment load monitoring programs provides little information on the mobilization, delivery and storage of sediments within the entire catchment. Thus, new approaches are required for improving the interpretation of basin sediment dynamics (Fryirs *et al*. 2007; Porto *et al*. 2013). Connectivity has recently emerged in Earth Surface and Environmental sciences, upon old questions (e.g. the sediment delivery problem; Walling 1983), as a useful concept for understanding the movement and spatiotemporal coupling of sediments between parts of the catchment. Sediment connectivity can be described as the active transfer of sediments from a source to a sink or the catchment outlet via soil particle/sediment detachment and transport,

100 which is affected by how the sediment moves between all geomorphic zones in the
101 catchment (Bracken *et al*. 2015). Sediment connectivity varies for each (and within each)
102 flood event in response to the highly dynamic nature of soil erosion, sediment transport
103 and deposition, which complicates process-based quantification and analysis
104 (Wainwright *et al*. 2011). In fact, attempts to measure (functional or process-based)
105 sediment connectivity explicitly are scarce and homogeneous analytical frameworks are
106 lacking (Letxartza-Artza & Wainwright 2011; Fryirs 2013; Bracken *et al*. 2015).

107 The use of fallout radioactive isotopes can provide important clues for sediment
108 tracing and connectivity analysis. Particularly, the fallout component of the lead-210
109 radioisotope (generally termed unsupported or excess lead-210, $^{210}Pb_{ex}$) has been very
110 valuable in a variety of applications during the last decades. $^{210}Pb_{ex}$ applications have
111 included the exploration of sedimentation rates in lakes, reservoirs, floodplains and other
112 sedimentary systems (Appleby & Oldfield 1978; Foster *et al*. 2007; Du & Walling 2012),
113 the analysis of soil erosion patterns (Mabit *et al*. 2010; Benmansour *et al*. 2013; Porto *et*
114 *al*. 2013) and spatial analysis of the processes of sediment transport and redistribution,
115 including sediment fingerprinting techniques (Collins *et al*. 1996; Walling 2005; Hancock
116 *et al*. 2014; Wilkinson *et al*. 2015; Estrany *et al*. 2016). Fallout lead-210 has a relatively
117 long half-life (22 years). It is deposited naturally, mostly through rainfall, on the soil
118 surface, where it is strongly adsorbed by clay-sized soil particles. Subsequent
119 redistribution of this fallout radionuclide across the landscape is mainly controlled by soil
120 erosion and sediment transport processes, which founds the basis for the broad potential
121 of $^{210}Pb_{ex}$ for soil and sediment tracing in terrestrial and aquatic environments (Walling
122 2003; Mabit *et al*. 2014). Recent applications of fallout lead-210 analysis for sediment
123 source tracing indicated that downstream transport, mixing and dilution of sediments can
124 obliterate the fallout radionuclide signal of sediment sources with low $^{210}Pb_{ex}$ initial

125 concentrations (e.g. large gullies and badlands), providing geomorphic evidence of
126 sediment (dis)connectivity (Wethered *et al*. 2015).

127 High measurement uncertainty (i.e. weight of analytical error over measured
128 values) and interference of sediment sampling/processing methods in radionuclide
129 determinations may, however, complicate the application of $^{210}Pb_{ex}$ for the assessment of
130 sediment redistribution processes, particularly in areas with highly erosive landforms
131 where radionuclide activities are usually low (Mabit *et al*. 2010; 2014; Dercon *et al*.
132 2012). In fact, the sampling methods and processing of sediments may influence particle-
133 size composition (Phillips *et al*. 2000; Soler *et al*. 2006; 2012; Regüés & Nadal-Romero
134 2012), a factor that affects considerably the concentration and measurement uncertainty
135 of fallout radionuclides (He & Walling 1996; Walling 2005; Smith & Blake 2014;
136 Foucher *et al*. 2015).

137 The aim of this work is to study the feasibility of using $^{210}Pb_{ex}$ analysis to assess
138 sediment connectivity in a small Mediterranean mountain basin with badlands (Vallcebre
139 catchments, Eastern Pyrenees). Our study approach is based on the analysis of the
140 spatiotemporal changes in the activity of fallout lead-210 for investigating sediment
141 (dis)connectivity between the badland areas and catchment streams, by applying $^{210}Pb_{ex}$
142 balance models for hypothesis generation and further experimental testing in the field.
143 We also evaluate the possible interferences and limitations of the sediment sampling
144 methods in our fallout radionuclide-based approach to sediment connectivity.

145 This paper is organized in two parts. First, after a brief description of the
146 experimental site, we present the conceptual underpinning and general sediment
147 connectivity hypotheses of the study. For this purpose, we use simple mass balance
148 models that simulate the spatiotemporal $^{210}Pb_{ex}$ signal of badland surface materials and
149 in-stream (transit) sediments in our experimental catchments. Second, we explore the

spatiotemporal patterns of sediment $^{210}Pb_{ex}$ activity empirically by a range of sampling methods (i.e. surface sediment traps, manual collection in streambeds, time-integrated and automated sampling of suspended sediments) in a variety of geomorphic sites (i.e. badland toes, stream transit sites, gauging stations), to assess spatial coupling of sediments across the basin and interpret the influence of the sediment sampling method on the radionuclide patterns analysed.

CHARACTERISTICS OF THE STUDY AREA: THE VALLCEBRE CATCHMENTS

The Vallcebre research catchments are located at the headwaters of the Llobregat River, in the Catalan Pyrenees, NE Spain (42º12'N, 1º49'E). The main cluster (Cal Rodó basin, Figure 1a) has an extension of 4.17 km^2 and an elevation gradient of 600 m (from 1,100 to 1,700 masl). The climate is Mediterranean humid. Mean annual air temperature is 9ºC; 16ºC in summer and 3ºC in winter, with approx. 40 days per year with mean air temperature below 0ºC. Mean annual precipitation is about 860 mm, with 90 rainy days per year on average and two wet periods (April-May and August-November) that account for about 70% of annual precipitation (Latron *et al*. 2009; Duvert *et al*. 2012). Precipitation characteristics have a seasonal pattern, with short storms of high rainfall intensity occurring in summer, and longer precipitation events of low to moderate intensity in autumn and spring. Snowfall accounts for less than 5% of annual precipitation (Gallart *et al*. 2013).

The research catchments lie on continental sedimentary bedrocks of Cretaceous-Paleocene age (*Garumnian* facies of the *Tremp* formation; Arostegui *et al*. 2011), dominated by smectite-rich mudstones that are susceptible to mass movements, erosion and badland formation (Solé *et al*. 1992; Moreno-de las Heras & Gallart 2016). Badlands extend over 2.8% of the surface of the Cal Rodó basin. These highly erosive landforms

175 are most widespread in the Ca l'Isard sub-basin (1.32 km^2 area contained within the Cal
176 Rodó basin), where they cover 4.5% of the catchment (Figures 1a and b). Elsewhere, the
177 basin is covered by pasture, Mediterranean shrubs and *Pinus sylvestris* forests. Forests
178 now cover about 60% of the area. During the last 60 years they have spontaneously spread
179 over old terraced agricultural fields due to land abandonment (Poyatos *et al*. 2003; Latron
180 *et al*. 2009).

181 Badland dynamics in the Vallcebre catchments follow a seasonal pattern of
182 regolith formation and erosion. Bedrock weathering takes place in winter due to repeated
183 freezing cycles, which lead to the development of highly erodible "popcorn" regolith
184 surfaces (Clotet *et al*. 1988; Regüés *et al*. 1995). Rill incision and erosion of the regolith
185 mantle are caused by high-intensity convective storms in summer. Typically, the eroded
186 sediments are straightaway transferred to the streams (i.e. badland slopes in the area are
187 rectilinear, generally lacking of significant sediment transport/storage layers such as large
188 slope toe concavities or major debris fans). Most of the sediment is, however, deposited
189 a short distance away due to low and ephemeral streamflow during summer (i.e. basin
190 runoff coefficients are usually about 1% in summer) and may remain stored from months
191 to years as streambed sediment deposits within the drainage network until long-lasting
192 autumn precipitations cause high runoff flow by means of saturation mechanisms (Gallart
193 *et al*. 2002; Latron *et al*. 2009; Gallart *et al*. 2013).

194 Erosion at the Vallcebre badlands has been explored during the last decades by a
195 variety of methods, i.e. short-term studies using erosion pins, plastic bags and Geib slot
196 divisors, extended 15-year model simulations using KINEROS2 and 40-year estimations
197 using a natural sediment trap. These gave an average erosion rate of 6-17 kg m^{-2} yr^{-1} or
198 an equivalent ~1 cm yr^{-1} mean denudation rate (Clotet *et al*. 1988; Castelltort 1995;
199 Martínez-Carreras *et al*. 2007; Gallart *et al*. 2013). Monitoring of badland surface

dynamics in the Vallcebre catchments indicated that their regolith mantle is hardly ever exhausted due to deep weathering caused by freezing, suggesting that badland erosion rates are essentially limited by rainfall energy (Regüés *et al*. 1995; Regüés & Gallart 2004). In contrast, sediment load and erosion rate at the basin scale are independent of rainfall energy and intensity. Rather, they are controlled by peak discharge, which is a function of rainfall depth and preceding soil moisture conditions (Soler *et al*. 2008; Duvert *et al*. 2012; Gallart *et al*. 2013). Decadal monitoring (1996-2009) of suspended sediment loads at the Vallcebre stream gauging stations provided catchment-scale annual erosion rates of 0.9 and 0.5 kg m^{-2} yr^{-1} for the Ca l'Isard sub-basin and Cal Rodó basin, respectively (Nord *et al*. 2010; Gallart *et al*. 2013).

HYPOTHESIS GENERATION USING $^{210}Pb_{ex}$ BALANCE MODELS

We apply two $^{210}Pb_{ex}$ balance models exploring (i) the temporal dynamics of badland regolith and sediment $^{210}Pb_{ex}$ activities, and (ii) the effects of in-stream sediment transit-time on the spatial patterns of $^{210}Pb_{ex}$ activity, to formulate a set of general sediment connectivity study hypotheses for the Vallcebre research catchments.

Badland regolith $^{210}Pb_{ex}$ activity model

A simple mass-balance model defining the $^{210}Pb_{ex}$ areal activity density at a stable reference site (A_{ref}, Bq m^{-2}) and at the end of a period of time (t, days) reflects the site activity density for the previous day (t-1), the $^{210}Pb_{ex}$ activity decay rate (λ=8.5 10^{-5} $days^{-1}$) and the $^{210}Pb_{ex}$ depositional input (or deposition flux). Assuming a steady (and essentially wet) deposition flux of fallout lead-210 (Appleby & Oldfield 1978; Mabit *et al*. 2014), the $^{210}Pb_{ex}$ depositional input can be calculated by the product of daily precipitation (P, mm day^{-1}) and mean lead-210 activity per precipitation unit (a, Bq L^{-1}):

$$A_{ref\,t} = A_{t-1}e^{-\lambda} + aP \quad (1)$$

A_{ref} in eq. 1 reaches equilibrium after 4-6 half-lives of lead-210 (about 90-140 years). However, $^{210}Pb_{ex}$ areal activity density for sites subjected to intense soil erosion, such as badlands, is far from equilibrium (Hancock *et al.* 2014; Wilkinson *et al*. 2015). On the assumption that each erosion event removes a layer of soil, and that depth distribution of $^{210}Pb_{ex}$ mass activity (Bq kg^{-1}) approaches a negative exponential form (Walling *et al*. 2003; Benmansour *et al*. 2013; Porto *et al*. 2013), the remaining $^{210}Pb_{ex}$ areal activity density of a site after the effects of an erosion event (*A(Er)*, Bq m^{-2}) can be calculated as (Walling *et al*. 2009):

$$A(Er) = A_{ref}\, e^{-\frac{Er}{h_0}} \quad (2)$$

where *Er* (kg m^{-2}) is the erosion rate of the event, and h_0 is the relaxation mass depth (or $^{210}Pb_{ex}$ penetration depth) that represents the depth above which 63% (i.e. 1-1/e) of total $^{210}Pb_{ex}$ is distributed.

By substituting A_{ref} in eq. 2, we can represent a daily-step $^{210}Pb_{ex}$ areal activity density balance model for a badland (regolith) site (*A*, Bq m^{-2}; Figure 2a):

$$A_t = (A_{t-1}e^{-\lambda} + aP)\, e^{-\frac{Er}{h_o}} \quad (3)$$

The loss of $^{210}Pb_{ex}$ areal activity density by soil erosion in the badland regolith (*Al*, Bq m^{-2}) can be determined by subtracting the activity before and after the erosion event (i.e. difference between eqs. 1 and 3):

$$Al_t = (A_{t-1}e^{-\lambda} + aP)(1 - e^{-\frac{Er}{h_0}}) \quad (4)$$

Modelled $^{210}Pb_{ex}$ mass activity of the eroded sediments (*Sa*, Bq kg^{-1}; Figure 2a) can be calculated from the areal activity density loss at the badland regolith (eq. 3) divided by the mass eroded per unit area:

$$Sa_t = \frac{(A_{t-1}e^{-\lambda} + aP)(1 - e^{-\frac{Er}{h_0}})}{Er} \quad (5)$$

Transit-time sediment $^{210}Pb_{ex}$ activity model

An equivalent formulation of the areal activity density $^{210}Pb_{ex}$ balance model presented in eq. 1 can be used to represent the (daily-step) transit variation of the sediment $^{210}Pb_{ex}$ mass activity (*TSa*, Bq kg^{-1}; Figure 2b) for sediments deposited in atmospherically exposed sediment stores within the stream network:

$$TSa_t = TSa_{t-1}e^{-\lambda} + \frac{F}{Bk} \quad (6)$$

where TSa_{t-1} (Bq kg^{-1}) is the mass activity of sediments deposited at time t-1 (days), λ is the $^{210}Pb_{ex}$ activity decay rate (8.5 10^{-5} days^{-1}), *F* is the $^{210}Pb_{ex}$ depositional input (Bq m^{-2} day^{-1}) and *Bk* is the blanket thickness of deposited sediments (kg m^{-2}).

Site simulations of $^{210}Pb_{ex}$ activity dynamics for badland surfaces and transit sediments

Site parameterization of the lead-210 atmospheric depositional input (or deposition flux) for the Vallcebre area is provided by the analysis of a reference $^{210}Pb_{ex}$ soil inventory (40 x 40 cm surface, 15 cm depth) in an undisturbed site (i.e. a natural meadow nearby the main badland areas) within the Cal Rodó basin (site location in Figure 1). $^{210}Pb_{ex}$ mass activity at the soil surface is 62 Bq kg^{-1} and decreases exponentially with depth (Figure 2c). Depth-integration of the soil $^{210}Pb_{ex}$ activity gives an areal density of 2,449 Bq m^{-2} (Figure 2c). Assuming a steady state balance between $^{210}Pb_{ex}$ input and decay, the reference soil inventory yields a depositional flux, *F*, of 0.21 Bq m^{-2} day^{-1} (76 Bq m^{-2} yr^{-1} annual flux), which is similar to the mean atmospheric flux of fallout lead-210 for the northwest coast of the Mediterranean basin (71 ± 27 Bq m^{-2} year^{-1}; Garcia-Orellana *et al*. 2006). Taking into consideration that fallout lead-210 flux is essentially controlled by wet deposition (Mabit *et al*. 2014) ^{210}Pb activity per precipitation unit, *a*, for the Vallcebre area (with a mean annual precipitation of 860 mm) can be calculated as 0.09 Bq L^{-1}.

The short fallout exposure duration of badland surface materials due to high erosion rates usually results in low $^{210}Pb_{ex}$ activity levels that are confined to the upper 1-2 cm of the regolith mantle (Hancock *et al*. 2014; Wilkinson *et al*. 2015). We, therefore, assume a small fallout lead-210 penetration for our regolith simulations, with a relaxation mass depth, h_0, of 8.3 kg m^{-2}, which is equivalent to a 1 cm depth for the average 1.2 g cm^{-3} regolith bulk density of the Vallcebre badland surface materials (Regüés *et al*. 1995). Detailed explorations of erosion dynamics for the Vallcebre badlands applying 3-year (1990-1993) experimental data from a small (1,240 m^2) badland area ("el Carot macro-plot"; Castelltort 1995) and extended 15-year (1994-2009) simulations using the event-oriented and physically-based KINEROS2 model (Martínez-Carreras *et al*. 2007; Gallart *et al*. 2013) indicated that the event-scale erosion rate correlates closely (Pearson's R= 0.85; 91 events) with the product of 5-minute maximum rainfall intensity and kinetic energy. Accordingly, the above-described regolith and sediment $^{210}Pb_{ex}$ activity models are fed by using a simple linear equation for calculating event badland erosion in the Vallcebre area (9% normalized root-mean-square error):

$$Er = 4.9\ 10^{-5} I_5\ K_e - 0.29 \qquad (7)$$

where Er (kg m^{-2}) is the event-scale badland erosion, I_5 (mm h^{-1}) is the maximum rainfall intensity in 5 minutes, and K_e (J m^{-2}) is the storm kinetic energy.

We applied local daily precipitation records (i.e. precipitation amount, storm I_5 and K_e) to simulate $^{210}Pb_{ex}$ activity for the Vallcebre badland regoliths during 2013 and 2014 in mass-balance equations 3 and 5, with a preceding model warming-up period of 18 months, which resulted in a saw-tooth seasonal pattern of excess lead-210 associated with the temporal patterns of rainfall characteristics (Figure 2d). Badland surface $^{210}Pb_{ex}$ activity increased from October to May, accumulating the fallout radionuclide flux generated by low-intensity rainfall events from autumn to spring. Conversely, regolith

299 $^{210}Pb_{ex}$ activity decreased from June to September, due to the erosive effect of high-
300 intensity summer storms, which were particularly active in July and August 2013 (with
301 I_5 and K_e reaching up to 94 mm h^{-1} and 1,500 J m^{-2}, respectively). Summer storms caused
302 a periodic reset of the badland regolith inventory, which resulted in maximum $^{210}Pb_{ex}$
303 activity levels below or near the lead-210 annual deposition flux for the study site (76 Bq
304 m^{-2}, Figure 2d). Simulated badland erosion for the modelled period was 14.2 kg m^{-2} yr^{-1},
305 with an equivalent badland denudation rate of 1.1 cm yr^{-1} that broadly matches long-term
306 estimations of badland erosion activity for the Vallcebre experimental area (Clotet *et al*.
307 1988; Gallart *et al*. 2013).

308 Simulation of transit-time influence on sediment $^{210}Pb_{ex}$ activity by using the
309 mass-balance equation 6 along with the Vallcebre fallout flux calculation (F, 0.21 Bq m^{-2}
310 day^{-1}) and three plausible sediment blanket thickness values reported for first-order
311 streams in Pyrenean catchments affected by badlands (Bk, 1, 5 and 10 kg m^{-2}; López-
312 Tarazón *et al*. 2011; Piqué *et al*. 2014) indicated a general increase in sediment $^{210}Pb_{ex}$
313 activity with increased in-stream residence time or age of the sediments (Figure 2e).
314 Sediment $^{210}Pb_{ex}$ activity increases were particularly important for the first years of stream
315 sediment storage, causing a sharp rise of modelled sediment activity after 2-5 years of in-
316 stream sediment residence of up to an order of magnitude for an initial sediment $^{210}Pb_{ex}$
317 concentration of 10 Bq m^{-2} and a blanket thickness of 1 kg m^{-2}. Similarly, empirical
318 estimations of sediment residence time by Wallbrink *et al*. (2002) for the Brisbane and
319 Logan rivers in Australia reflected a sharp increase in sediment $^{210}Pb_{ex}$ activity within 2-
320 5 years of in-stream storage, which also suggests that, for simple channels, accumulation
321 of fallout 210-lead in sediments may increase downstream with sediment age.

322

323 *Formulation of sediment connectivity hypotheses for the Vallcebre research catchments*

Our $^{210}Pb_{ex}$ balance models for the Vallcebre research catchments suggested: (i) a saw-tooth temporal pattern of sediment $^{210}Pb_{ex}$ activity in the sediment sources (i.e. the badland surfaces) due to the accumulation of fallout lead-210 because of low-intensity autumn and winter rainfalls, and subsequent $^{210}Pb_{ex}$ loss caused by highly erosive summer storms, and (ii) an increase in sediment $^{210}Pb_{ex}$ activity with in-stream sediment storage/age. Geomorphic evidence for spatiotemporal changes in the activity of fallout radionuclides provides a ready approach for assessing sediment (dis)connectivity between sediment sources and basin streams (Wethered *et al*. 2015). Accordingly, we hypothesize that:

(i) Spatial sediment coupling between badland sites and basin streams is reflected by the conservation of the modelled (saw-tooth) seasonal pattern of badland surface $^{210}Pb_{ex}$ activity in the suspended sediments of the streams.

(ii) Storage of fine sediments within the streambeds results in downstream increases in sediment $^{210}Pb_{ex}$ activity, also reflecting temporal decoupling between the production of sediments at their sources (i.e. badland surface) and the mobilization of sediments in the basin streams.

METHODS FOR HYPOTHESIS TESTING

Sediment sampling and laboratory analyses

Sediment sampling took place during 2013 and 2014 at a variety of basin locations along a 1.5 km section of the Torrent del Purgatori, a first-order stream connecting the most significant badland areas of the Vallcebre catchments with the outlets of the Ca l'Isard sub-basin and the Cal Rodó basin (Figure 1a). The locations included the slope toe of a badland site at the head of the stream, downstream places at stream transit sites, and two automated gauging stations at the outlet of Ca l'Isard and Cal Rodó. Sediments were

sampled by a range of methods: (a) a surface trap (permeable bag) of sediments at the toe of the badland site (Figures 1a and 1c), (b) direct collection of (2-3 cm depth) sediments from streambed deposits at three stream transit sites (at 100-300 m and 1.3 km downstream from the badland site) and the two gauging stations (Figures 1a and 1d), (c) five time-integrated sediment samplers (following the design of Phillips *et al*. 2000) at the same five (stream transit and gauging station) locations (Figures 1a and 1e), and (d) two automated (*ISCO*) sequential water samplers with high-frequency acquisition (as much as one sample every 2 mins during high-discharge events) of (1 litre) water and suspended sediment samples at the two gauging stations (Figures 1a and 1f). Because of the transient character of the flow in the streams studied, the time-integrated samplers were installed in nearly dry streambeds (Figure 1e). Consequently, their original design was slightly modified by piercing three (2 mm) air escape holes in the upper part of the samplers to facilitate the filling of the tubes at the beginning of the events. Complementary data for the calculation of catchment-scale sediment yield during the study period was provided by monitoring sediment load at the Ca l'Isard and Cal Rodó gauging stations in continuous by means of automated turbidity (*D&A OBS3*) and ultrasonic (*Bestobell-Mobrey MSM40*) suspended sediment sensors (Soler *et al*. 2012; Gallart *et al*. 2013).

A total of 50 sediment samples were collected during the study period, encompassing 11 badland sediment samples from the surface trap (taken from April to December 2014), 7 streambed sediment samples (taken from April to May 2014), 16 suspended sediment samples from the automated (*ISCO*) sequential samplers (taken from March 2013 to December 2014, and integrated over consecutive runoff events to reach a minimum size of 50-100 g of dry matter for laboratory analysis), and 17 suspended sediment samples from the time-integrated samplers (taken from June to December

2014). The samples were taken to the laboratory and oven-dried at 65ºC. Both sequential and time-integrated sediment samples were recovered by means of sedimentation. Previous field observations of sediment dynamics in the Vallcebre catchments indicated that peak streamflow transports significant amounts of poorly weathered particles of mudstone in suspension, which can be strongly altered by sediment pre-processing in the laboratory (Soler *et al*. 2012). To preserve the original physical characteristics of the sediments, no sieving or sediment fractioning was applied. Absolute grain-size composition and specific surface area (SSA, m^2g^{-1}) for all the samples was measured by a laser-diffraction analyser (*Malvern Mastersizer 2000*).

Total ^{210}Pb and ^{226}Ra (from ^{214}Bi) activity (Bq kg^{-1}) was measured by gamma spectrometry (gamma-ray emissions at 46.5 and 609.3 keV, respectively) using an iron-shielded, high-purity coaxial germanium detector (*Canberra GR5023-7500 SL*). Spectra were acquired and analysed by the *Canberra GENIE 2000* software. Energy and efficiency calibrations were performed by certified gamma cocktail standards purchased from the Spanish Research Centre for Energy, Environment and Technology (CIEMAT). Counting time applied for gamma spectrometry was 86,400 s for all samples, obtaining a data precision range of 10-20% at the 95% confidence level. Prior to analysis, all samples were sealed in polyethylene bottles for 21 days to achieve equilibrium between ^{226}Ra and its daughter ^{222}Rn (1,622 years and 4 days half-life, respectively). $^{210}Pb_{ex}$ activity for each sample was determined by subtracting the supported lead-210 in equilibrium with ^{226}Ra from the total ^{210}Pb activity. Measured ^{226}Ra activity values were corrected (~0.8 factor) for the calculation of *in situ* ^{226}Ra-supported ^{210}Pb concentrations, based on the ratio of total ^{210}Pb to (uncorrected) ^{226}Ra observed in the lower part (i.e. depth >10 cm) of our reference $^{210}Pb_{ex}$ soil inventory, where $^{210}Pb_{ex}$ was assumed to be absent (cf. Graunstein & Turekian 1986; Wallbrink & Murray 1996; Porto *et al*. 2013; Mabit *et al*. 2014).

399 Uncertainty in the determination of $^{210}Pb_{ex}$ was highly variable, with analytical error
400 ranging from 10% to over 100% of measured activity values. $^{210}Pb_{ex}$ activity may take
401 negative values for sediment (or soil) samples where total ^{210}Pb and ^{226}Ra-supported ^{210}Pb
402 show similar concentrations and are affected by high measurement uncertainty levels
403 (Mabit *et al*. 2010). Negative $^{210}Pb_{ex}$ activity measurements in this study were taken as
404 zero for purposes of data analysis.
405
406 *Data analysis*
407 We tested for the effects of the sediment sampling method and its relation with particle-
408 size distribution (i.e. median grain size d50, and SSA) on experimental sediment $^{210}Pb_{ex}$
409 activity and its associated measurement uncertainties, by applying Kruskall-Wallis
410 ANOVA to the full experimental set of 50 sediment samples. $^{210}Pb_{ex}$ activity data with
411 analytical error above 100% of measured value were subsequently discarded for the
412 evaluation of the sediment connectivity hypotheses.
413 The temporal pattern of experimental $^{210}Pb_{ex}$ activity in sediments was evaluated
414 against the simulated (saw-tooth) seasonal dynamics of fallout radionuclide activities for
415 the badland surfaces to ascertain spatial coupling (by pattern conservation of fallout
416 radionuclide concentrations) between the badland regoliths and the sediments in the basin
417 streams. Comparison of radionuclide concentrations between source materials (e.g. soils,
418 regoliths) and sediments generally reflects sediment enrichment ratios due to strong
419 radionuclide binding to the most mobile, fine-grained particles, which requires the
420 application of particle-size corrections for exploring source-stream sediment radionuclide
421 distribution patterns (Collins *et al*. 1996; He & Walling 1996; Walling 2005; Smith &
422 Blake 2014). The simulated $^{210}Pb_{ex}$ activities at the badland surfaces were, therefore,

423 particle-size corrected for comparison with the experimental $^{210}Pb_{ex}$ in sediments using
424 the following conversion equation (He & Walling 1996; Porto *et al*. 2003):

425 $$C_C = \left({S_S}/{S_R}\right)^n C_0 \quad (8)$$

426 where C_0 is the original (simulated) $^{210}Pb_{ex}$ activity for sediments generated at the badland
427 surface, C_C is the corrected $^{210}Pb_{ex}$ activity value, S_S is the mean SSA for the experimental
428 sediments applied in the evaluation, S_R is the typical SSA for the badland regoliths, and
429 n is a scaling exponent. We used the minimum SSA measured for the 11 sediment samples
430 collected at the badland toe location (surface sediment trap), as a conservative estimate
431 of the particle size for the original regolith materials at the badland surface, S_R. A value
432 of 0.75 was applied to the scaling exponent, n, which is within the range of empirical
433 values reported by He & Walling (1996) for the correction of soil/sediment $^{210}Pb_{ex}$
434 measurements.

435 Temporal (month to year) (dis)connection between the sediment production at
436 the badland surfaces and the mobilization of sediments in the basin streams was assessed
437 by analysing downstream patterns of sediment $^{210}Pb_{ex}$ activity with a general linear mixed
438 model (GLMM). The GLMM included (i) the downstream distance for the sediment
439 sampling locations along the Torrent del Purgatori as a continuous fixed predictor of
440 sediment $^{210}Pb_{ex}$ activity, and (ii) the sampling site as a random factor for analysis across
441 monitored runoff/sediment transport events.

442

443 RESULTS AND DISCUSSION

444 *Effects of sampling method on sediment characteristics and $^{210}Pb_{ex}$ activity patterns*

445 Our results show a strong effect of sampling method on the physical characteristics of
446 sediments. Suspended sediments showed a smaller median (d50) grain size and larger
447 SSA than deposited sediments collected at either the badland site (surface trap) or the

448 streambed (Figures 3a and b), which reflects general differences in the nature (i.e.
449 suspended *versus* deposited) of sediments. In addition, suspended sediments collected by
450 the sequential (*ISCO*) samplers were significantly finer than those collected by the time-
451 integrated samplers (Figures 3a and b), which suggests physical interference of sediment
452 sampling instruments with the sediment characteristics. In fact, at the scale of individual
453 runoff events, sediments collected by the time-integrated samplers at the gauging stations
454 showed d50 grain sizes 42-102% bigger than those collected by the sequential (*ISCO*)
455 samplers at the same locations. Accordingly, Phillips *et al*. (2000) demonstrated that the
456 application of time-integrated samplers for collecting suspended sediments may increase
457 their median grain size by a 40-150% range, depending on flow velocity and original
458 particle-size distribution. On the contrary, previous experimental comparisons of
459 suspended sediment concentration and grain size by using automated and simultaneous
460 control samples from the Vallcebre catchments indicated that the original grain-size
461 distributions of suspended sediments were satisfactorily captured by the time-integrated
462 (*ISCO*) samplers (Soler *et al*. 2006).

463 Mean sediment $^{210}Pb_{ex}$ activity was in general low, ranging from 0 to about 10 Bq
464 kg^{-1} for the variety of sampling methods (Figure 3c), which reflects the fresh rock origin
465 of the sediments, but also evidences a very strong influence of sampling methods and
466 sediment physical characteristics on radionuclide concentrations. In fact, the finer,
467 suspended sediments that were retrieved by the sequential (*ISCO*) samplers showed
468 higher radionuclide activities than the coarser suspended sediments retained by the time-
469 integrated samplers. Furthermore, $^{210}Pb_{ex}$ activity for the coarse-grained, deposited
470 sediments that were collected from the badland sediment bag and the streambed locations
471 showed zero and near-zero values (Figure 3c). Measurement uncertainty severely affected
472 the $^{210}Pb_{ex}$ data. $^{210}Pb_{ex}$ analytical error was above 100% of the measured value for all

473 data except 16 measurements, all of which corresponded to suspended sediment samples
474 of median grain size ranging from 5 to 20 μm (Figure 3d).

475 The impact of sediment particle-size distribution on $^{210}Pb_{ex}$ measurements can be
476 explained by the selective adsorption of lead-210 by the finer, clay-sized mineral particles
477 of soils and sediments (He & Walling 1996; Mabit *et al*. 2014; Foucher *et al*. 2015). A
478 common method designed to mitigate differences in particle-size distribution for
479 radionuclide analysis consists of isolating the <63 μm fraction of the soils and sediments
480 (Walling 2005). Our results, however, indicate that $^{210}Pb_{ex}$ concentrations are only
481 detectable for sediments with median grain size below 20 μm (Figure 3d). Other studies
482 have suggested the application of wet fractioning of sediments by particle settling and
483 flocculation to isolate <10 μm grains for radionuclide analysis, particularly in catchments
484 where sediment transport is dominated by clay-sized particles (Olley & Caitcheon 2000;
485 Hancock *et al*. 2014; Wilkinson et al. 2015). Nonetheless, wet fractioning of sediments is
486 undesirable in areas with badlands developed over friable and/or soft materials (e.g. marls
487 and mudstone), where particle-size distribution may behave as a dynamic sediment
488 property that can be strongly altered by sediment processing in the laboratory. For
489 example, observations in the Vallcebre catchments and similar highly erosive mountain
490 basins with badlands indicated that large floods typically transport significant proportions
491 of poorly weathered, sand-grained particles of soft bedrock in suspension, which may be
492 further weathered into new fine sediments in a variable time after deposition on the
493 streambed or by intense sediment manipulation in the laboratory (Mathys *et al*. 2003;
494 Soler *et al*. 2008, 2012; Regüés and Nadal-Romero 2012).

495 The dynamic nature of badland-originated sediments (i.e. radionuclide-
496 unlabelled, coarse sediments may decay into fine particles by intensive sediment
497 processing in the laboratory) and the strong influence of physical sediment characteristics

(i.e. particle-size distribution) on both radionuclide activity and measurement uncertainty patterns stress the importance of selecting efficient methods for fine sediment sampling and investigation in highly erosive catchments with marly and mudstone badlands, where $^{210}Pb_{ex}$ concentrations are low and strongly influenced by high levels of analytical error. Our experimental results at the Vallcebre catchments suggest that the automatic sequential water samplers provide the best method for collecting representative samples (in terms of particle-size distribution) of fine, suspended sediments for implementing sediment tracing by radionuclide analysis in areas with very active badlands developed over soft bedrock. Additionally, the application of counting times longer than that used in this study (86,400 s) for deriving sediment $^{210}Pb_{ex}$ concentration estimates from gamma spectrometry or the use of alternative analytical methodologies with higher precision for the detection of low radionuclide activity levels (e.g. alpha spectrometry; Mabit *et al*. 2008) may help to minimize the uncertainty associated to the sediment $^{210}Pb_{ex}$ determinations.

Assessing catchment sediment connectivity: sediment load and spatiotemporal patterns of suspended sediment $^{210}Pb_{ex}$ activity

Suspended sediment load during the study period totalled 1,370 Mg for Ca l'Isard and 1,875 Mg for Cal Rodó, representing 0.52 and 0.23 kg m^{-2} yr^{-1} sediment yield at the sub-basin and basin scales, respectively. These figures are about 50% below the long-term mean sediment yield records for the Vallcebre catchments (0.9 and 0.5 kg m^{-2} yr^{-1} for Ca l'Isard and Cal Rodó, respectively; Nord *et al*. 2010; Gallart *et al*. 2013), and contrast considerably with the deep badland denudation estimate obtained in our simulation results for 2013 and 2014 (1.1 cm yr^{-1}). This variation in erosive performance between the catchment and badland sites for the study period can be explained by the local dynamics

523 of precipitation, which suggests low sediment transport capacity at the sub-basin and
524 basin scales in 2013 and 2014. In fact, 2013-2014 precipitation (910 mm yr^{-1}) was 6%
525 above the historical average records, with regular activity of high-intensity summer
526 storms, which strongly control badland erosion rates in the study area (Castelltort 1995;
527 Martinez-Carreras *et al*. 2007; Gallart *et al*. 2013). The long-lasting autumn precipitations
528 that regulate suspended sediment load in the Vallcebre streams (Soler *et al*. 2008; Gallart
529 *et al*. 2013) were, in turn, 40% below the mean historical rainfall amount, resulting in
530 limited sediment transport at the broader catchment scale. Accordingly, downscaling of
531 the 2013-14 sediment yield records obtained at the Ca l'Isard and Cal Rodó gauging
532 stations over the total badland extension for the Vallcebre catchments (11.7 ha) results in
533 a figure 30-40% below the simulated badland erosion rate for the study period. These
534 results suggest that significant amounts of fresh badland sediments remained stored
535 within the stream network during the study period, which was also confirmed by direct
536 observation of streambed deposits in the field.

537 The analysis of spatiotemporal patterns of sediment fallout radionuclide
538 concentrations can facilitate the assessment of active connections and transit-time
539 dynamics of sediments between parts of the catchment (Wallbrink *et al*. 2002; Walling
540 2005; Belmont *et al*. 2014; Wethered *et al*. 2015). The group of experimental sediment
541 samples unaffected by severe $^{210}Pb_{ex}$ measurement uncertainty (i.e. suspended sediments
542 with homogeneous 5-20 μm median grain size) showed $^{210}Pb_{ex}$ activity levels ranging
543 from 7 to about 25 Bq kg^{-1} during the study period, which overall matches simulated
544 radionuclide concentrations (Figure 4a). More importantly, the temporal variations in
545 experimental $^{210}Pb_{ex}$ sediment activity reproduced the simulated temporal pattern of
546 fallout lead-210 for sediments generated at the badland surfaces. In fact, $^{210}Pb_{ex}$ activity
547 in the experimental sediments tracked the characteristic (saw-tooth) seasonal pattern of

548 fallout radionuclide concentrations modelled for the badland regoliths, which predicted a
549 build-up of $^{210}Pb_{ex}$ activity at the badland regoliths due to low-intensity precipitation
550 events in autumn and spring, and a subsequent $^{210}Pb_{ex}$ depletion caused by high-intensity
551 showers in summer (Figures 2d and 4a). As expected, the drop in measured suspended
552 sediment $^{210}Pb_{ex}$ activity levels was particularly pronounced during July and August
553 2013, when strong summer storms with intensities up to 94 mm h^{-1} in five minutes caused
554 deep erosion at the badland sites. The close similarity of both the simulated and the
555 experimental sediment radionuclide activity patterns discard any significant contributions
556 of sediments from other surface cover types, such as the very stable pastures and forests
557 of the Vallcebre catchments, where soil $^{210}Pb_{ex}$ patterns can be assumed to be in
558 equilibrium at activity levels of about 60 Bq kg^{-1} at the soil surface (Figure 2c). These
559 results agree with previous sediment budget investigations in the Vallcebre catchments,
560 which revealed the badland surfaces as the ruling source to basin sediment load (Gallart
561 *et al*. 2002; 2013; Soler *et al*. 2008).

562 The observed conservation of the modelled seasonal arrangement of badland
563 regolith $^{210}Pb_{ex}$ concentrations in the radionuclide signatures of collected suspended
564 sediment samples (Figure 4a) indicates high fine sediment connectivity between the
565 badland sites, the streams and the outlet of the Vallcebre catchments. Similarly, a broad
566 range of sediment studies in small (i.e. less than 50 km^2) Mediterranean mountain basins
567 across the Pyrenees and Central Alps have highlighted a high connectivity and fast stream
568 transmission of fine sediments originating in highly dynamic humid badlands, especially
569 for areas where these erosive landforms are structurally integrated in the basin stream
570 network (Descroix & Mathys 2003; Francke et al. 2008; Nadal-Romero *et al*. 2008;
571 Duvert et al. 2012; Gallart et al. 2013). At the larger regional scale, the high mobility of
572 fine sediments generated in these badland landscapes can result in the delivery of large

amounts of suspended sediments through the drainage networks. For example, sediment budget investigations and spectral fingerprinting analysis of suspended sediment transport for the Isabena basin, a central Pyrenean 445-km^2 basin affected by (about 1% of terrain) badlands, reflected a yearly average input of about 260,000 t y^{-1} badland sediments and a 60-80% sediment delivery ratio (López-Tarazón *et al*. 2012; Brosinsky *et al*. 2014). Similarly, for the mesoscale regional context of the Vallcebre catchments (i.e. the upper Llobregat basin; 500 km^2) where badlands represent ~0.5% of the terrain, integrated sediment budget and GIS analysis estimated badland sediment contribution to represent up to 30% of the regional flux of suspended sediments (Clotet *et al*. 1984; Moreno-de las Heras *et al*. 2016).

Unlike the downstream sediment $^{210}Pb_{ex}$ concentration increase with sediment age suggested by our transit-time sediment simulations (Figure 2e), fallout lead-210 activity levels for the experimental suspended sediments decreased downstream between the sampling locations of the Vallcebre catchments (Figure 4b). A variety of studies have explained downstream decreases in the $^{210}Pb_{ex}$ concentrations of suspended sediments by the contribution of unlabelled fresh materials from (nearly vertical) streambanks showing nil or little fallout lead-210 interception (Belmont *et al*. 2014; Hancock *et al*. 2014; Wethered *et al*. 2015). Channel entrenchment in the Vallcebre catchments is strongly conditioned by the occurrence of infrequent, strong autumn events with an approx. 5-year return period (Gallart *et al*. 2002, 2013). Nonetheless, the observed low sediment transport conditions for 2013 and 2014 did not support streambank erosive activity during the study period. More likely, flushing of the most dynamic, fine sediments from the streambed by flooding may have prevented $^{210}Pb_{ex}$ accumulation in temporary sediment stores within the stream network. Decay of poorly weathered sand-grained particles of clayey bedrock stored in streambed deposits into fine particles may also add radionuclide-

598 unlabelled suspended sediments to the streamflow (Soler *et al*. 2012), contributing to the
599 observed downstream reduction in sediment $^{210}Pb_{ex}$ activity. These results must, however,
600 be explored with caution due to the scarcity of events with paired observations between
601 sediment sampling locations with reliable sediment $^{210}Pb_{ex}$ measurements in our data.
602 More information is required, optimally for a wide variety of streamflow conditions (e.g.
603 low, regular and extreme runoff events), to disentangle the complex interactions that
604 control the downstream dynamics of sediment $^{210}Pb_{ex}$ concentration. In the light provided
605 by our results, we hypothesize that high streamflow conditions that dramatically activate
606 the mobilization of long-term sediment stores and general channel entrenchment in the
607 drainage network (Gallart & Clotet 1988; Gallart *et al*. 2013; Serrano-Muela *et al*. 2015)
608 will exacerbate the downstream obliteration of the suspended sediment $^{210}Pb_{ex}$ signatures.
609 Process-based understanding of sediment connectivity (i.e. the continuity of
610 sediment transfer between different zones of a catchment; Bracken *et al*. 2015) is required
611 for effective basin management, particularly in Mediterranean mountain basins, where
612 badland occurrence is a common phenomenon that can have important consequences for
613 river dynamics, freshwater ecosystems and the security of water resources. Despite very
614 intense discussion in a series of recent conceptual studies (e.g. Bracken & Croke 2007;
615 Lexartza-Artza & Wainwright 2011; Wainwright *et al*. 2011; Bracken *et al*. 2015; Okin
616 *et al*. 2015) there is little consensus about how to quantify sediment connectivity. A broad
617 range of studies carried out in Mediterranean mountain basins with badlands have applied
618 the sediment budget approach, which rely on the measurement, extrapolation and
619 accumulation of sediment production/transport in different parts of the catchment to infer
620 sediment transfer (Clotet 1984; Llorens *et al*. 1997; Nadal-Romero *et al*. 2008; López-
621 Tarazón *et al*. 2012; Gallart *et al*. 2013). In this context, the use of environmental tracers,
622 such as the fallout component of the radioactive isotope lead-210, has provided alternative

623 methodologies for inferring sediment transfer in a variety of environments (e.g. Walling
624 2005; Porto *et al*. 2013; Wilkinson *et al*. 2015; Estrany *et al*. 2016). Radioisotope
625 sediment studies are, however, notably lacking in badland environments, where their
626 highly erosive nature is frequently perceived as a major limitation for $^{210}Pb_{ex}$ analysis
627 (Mabit *et al*. 2008; Dercon *et al*. 2012). Differently, our study indicates that the highly
628 dynamic nature of mountain Mediterranean badlands provides an opportunity for the
629 assessment of sediment connectivity on the basis of fallout lead-210 activity patterns. In
630 fact, badland surface $^{210}Pb_{ex}$ activity is characterized by a seasonal pattern (i.e.
631 progressive accumulation in autumn/winter followed by a sharp summer reduction of
632 fallout levels) that can be used to track the continuity of sediment transfer between
633 different parts of the catchment by spatiotemporal analysis of sediment $^{210}Pb_{ex}$
634 concentration. Overall, our study reveals sediment $^{210}Pb_{ex}$ analysis as a powerful tool that
635 can complement more traditional sediment load monitoring programs for the study of fine
636 sediment connectivity in Mediterranean basins affected by the activity of highly erosive
637 landforms.
638
639 CONCLUSIONS
640 This work provides empirical evidence of the feasibility of using excess lead-210 analysis
641 to study sediment connectivity in Mediterranean basins affected by badland dynamics,
642 and also illustrates the analytical difficulties of the sediment $^{210}Pb_{ex}$ approach (in relation
643 to sediment characteristics and sampling method) for catchments where the sediment
644 dynamics are strongly controlled by highly erosive landforms over soft bedrock. Both
645 deposited and suspended sediments collected at the Vallcebre catchments showed, in
646 general, low sediment $^{210}Pb_{ex}$ concentrations, illustrating their fresh-rock origin at the
647 badland sites, but also hampering the understanding of sediment $^{210}Pb_{ex}$ patterns due to

high measurement uncertainty (particularly for sediments with d50>20μm) and to strong dependence on sediment sampling methodology. Application of mass balance models for exploring the spatiotemporal patterns of sediment $^{210}Pb_{ex}$ signatures demonstrated that the fine, suspended sediments collected at the Vallcebre streams showed a saw-tooth pattern of $^{210}Pb_{ex}$ activity that mimics the seasonal cycles of (autumn to springtime) lead-210 fallout accumulation and subsequent erosion by summer storms at the badland sites. Contrary to the in-stream transit increases of sediment $^{210}Pb_{ex}$ activity that were predicted by our model simulations, fallout lead-210 concentrations in the suspended sediments decreased towards the basin outlet, suggesting that fine sediment flushing by flooding prevented $^{210}Pb_{ex}$ accumulation in the coarser streambed sediment deposits. These results indicate very high fine-sediment connectivity between the badlands, streams and basin outlet of the Vallcebre catchments, as well as the fast transmission of fallout lead-210 by the finest and most dynamic fraction of sediments. Conversely, a significant fraction of fresh sediments eroded from badland surfaces are sandy or coarser and untagged by the fallout; the connectivity of these sediments appears to be much lower, as they manly remain in the streambed and their decay into finer particles contributes to the bulk sediment load during major sediment load events. This study was carried out during a period with relatively low sediment transport capacity and characterized by the build-up of temporal streambed deposits of coarse sediments. Further research is required to analyse the influence on the spatiotemporal sediment $^{210}Pb_{ex}$ patterns studied of low-recurrence, high-flow events that mobilize long-term sediment stores from the streambeds.

AKNOWLEDGEMENTS

672 This study was supported by the research projects MEDhyCON (CGL2012-32446) and
673 EcoHyMed (CGL2013-43418-R) funded by the Spanish Ministry of Economy and
674 Competitiveness (MINECO). Mariano Moreno-de las Heras is beneficiary of a Beatriu
675 de Pinós fellowship (SEDCONMED, 2014 BP-B 00111) co-funded by the Generalitat de
676 Catalunya and the European Commission. Fieldwork and laboratory support by Diego
677 Vuolo and members of the Surface Hydrology and Erosion group (SHEg, IDAEA-CSIC),
678 the Mediterranean Ecogeomorphological and Hydrological Connectivity Research team
679 (MEDhyCON, University of the Balearic Islands) and the Environmental Radioactivity
680 Laboratory (LaboRA, University of the Balearic Islands) are gratefully acknowledged.
681 We also thank the editor, Saskia Keesstra, and four anonymous reviewers for their
682 thoughtful comments.
683
684 REFERENCES
685 Appleby PG, Oldfield F. 1978. The calculation of lead-210 dates assuming a constant rate
686 supply of unsupported ^{210}Pb to the sediment. *Catena* **5:** 1-8. DOI: 10.1016/S0341-
687 8162(78)80002-2.
688 Arostegui J, Baceta JI, Pujalte V, Carrecedo M. 2011. Late Cretaceous-Paleocene mid-
689 latitude climates: inferences from clay mineralogy of continental-coastal sequences
690 (Tremp-Graus area, southern Pyrenees, N Spain). *Clay Minerals* **46:** 105-126. DOI:
691 10.1180/claymin.2011.046.1.105.
692 Belmont P, Willenbring JK, Schottler SP, Marquard J, Kumarasamy K, Hemmis JM.
693 2014. Toward generalizable sediment fingerprinting with tracers that are conservative
694 and nonconservative over sediment routing timescales. *Journal of Soils and Sediments*
695 **14:** 1479-1492. DOI: 10.1007/s11368-014-0913-5.

Benmansour M, Mabit L, Nouira A, Moussadek R, Bouksirate H, Duchemin M, Benkdad A. 2013. Assessment of soil erosion and deposition rates in a Moroccan agricultural field using fallout ^{137}Cs and $^{210}Pb_{ex}$. *Journal of Environmental Radioactivity* **115:** 97-116. DOI:10.1016/j.jenvrad.2012.07.013.

Bracken LJ, Croke J. 2007. The concept of hydrological connectivity and its contribution to understanding runoff dominated geomorphic systems. *Hydrological Processes* **21:** 1749-1763. DOI:10.1002/hyp.6313.

Bracken LJ, Turnbull L, Wainwright J, Bogaart P. 2015. Sediment connectivity: a framework for understanding sediment transfer at multiple scales. *Earth Surface Processes and Landforms* **40:** 177-188. DOI: 10.1002/esp.3635.

Brosinsky A, Foerster S, Segl K, López-Tarazón JA, Piqué G, Bronstert A. 2014. Spectral fingerprinting: characterizing suspended sediment sources by the use of VNIR-SWIR spectral information. *Journal of Soil and Sediments* **14:** 1965-1981. DOI: 10.1007/s11368-014-0927-z.

Castelltort X. 1995. *Erosió, transport i sedimentació fluvial com a integració dels processos geomorfològics d'una conca (conca de Cal Rodó)*. PhD Thesis, Universitat de Barcelona, Barcelona.

Clotet N. 1984. La Conca de la Baells (Alt Llobregat): Els processos geomorfològics actuals responsables del subministrament de sòlids i blanç previ de sediments. *Acta Geológica Hispanica* **19:** 177-191.

Clotet N, Gallart F, Balasch C. 1988. Medium-term erosion rates in a small scarcely vegetated catchment in the Pyrenees. *Catena Supplement* **13:** 37-47.

Collins AL, Walling DE, Leeks GJL. 1996. Composite fingerprinting of the spatial source of fluvial suspended sediment: a case study of the Exe and Severn river basins, United Kingdom. *Géomorphologie* **2:** 41-53. DOI: 10.3406/morfo.1996.877.

721 Dercon G, Mabit L, Hancock G, Nguyen ML, Dornhofer P, Bacchi OOS, Benmansour
722 M, Bernard C, Froehlich, Golosov VN, Haciyakupoglu S, Hai PS, Li Y, Lobb DA,
723 Onda Y, Popa N, Rafiq M, Ritchie JC, Schuller P, Shakhashiro A, Wallbrink P,
724 Walling DE, Zapata F, Zhang X. 2012. Fallout radionuclide-based techniques for
725 assessing the impact of soil conservation measures on erosion control and soil quality:
726 an overview of the main lessons learnt under an FAO/IAEA Coordinated Research
727 Project. *Journal of Environmental Radioactivity* **107:** 78-85.
728 DOI:10.1016/j.jenvrad.2012.01.008.
729 Descroix L, Mathys N. 2003. Processes, spatio-temporal factors and measurements of
730 current erosion rates in the French Southern Alps: A review. *Earth Surface Processes*
731 *and Landforms* **28:** 993-1011. DOI:10.1002/esp.514.
732 Du P, Walling DE. 2012. Using ^{210}Pb measurements to estimate sedimentation rates on
733 river floodplains. *Journal of Environmental Radioactivity* **103:** 59-75.
734 DOI:10.1016/j.jenvrad.2011.08.006.
735 Duvert C, Nord G, Gratiot N, Navratil O, Nadal-Romero E, Mathys N, Némery J, Regüés
736 D, García-Ruiz JM, Gallart F, Esteves M. 2012. Towards prediction of suspended
737 sediment yield from peak discharge in small erodible mountainous catchments (0.45-
738 22 km^2) of France, Mexico and Spain. *Journal of Hydrology* **454-455:** 42-55.
739 DOI:10.1016/j.jhydrol.2012.05.048.
740 Estrany J, López-Tarazón JA, Smith HG. 2016. Wildfire effects on suspended sediment
741 delivery quantified using fallout radionuclide tracers in a Mediterranean catchment.
742 *Land Degradation and Development* **27:** 1501-1512. DOI:10.1002/ldr.2462.
743 Foster IDL, Boardman J, Keay-Bright J. Sediment tracing and environmental history for
744 two small catchments, Karoo Uplands, South Africa. *Geomorphology* **90:** 126-143.
745 DOI:10.1016/j.geomorph.2007.01.011.

746 Foucher A, Laceby PJ, Salvador-Blanes S, Evrad O, Le Gall M, Lefèvre I, Cerdan O,
747 Rajkumar V, Desmet M. 2015. Quantifying the dominant sources of sediment in a
748 drained lowland agricultural catchment: The application of a Thorium-based particle
749 size correction in sediment fingerprinting. *Geomorphology* **250:** 271-281.
750 DOI:10.1016/j.geomorph.2015.09.007.
751 Francke T., López-Tarazón J.A., Vericat D., Bronstert A., Batalla R.J. 2008. Flood-based
752 analysis of high magnitude sediment transport using a non-parametric method. *Earth*
753 *Surface Processes and Landforms* **33:** 2064-2077. DOI:10.1002/esp.1654.
754 Fryirs KA. 2013. (Dis)Connectivity in catchment sediment cascades: a fresh look at the
755 sediment delivery problem. *Earth Surface Processes and Landforms* **38:** 30-46.
756 DOI:10.1002/esp.3242.
757 Fryirs KA, Brierley GJ, Preston NJ, Kasai M. 2007. Buffers, barriers and blankets: The
758 (dis)connectivity of catchment-scale sediment cascades. *Catena* **70:** 49-67.
759 DOI:10.1016/j.catena.2006.07.007.
760 Gallart F, Clotet N. 1988. Some aspects of the geomorphic processes triggered by an
761 extreme rainfall event: the November 1982 flood in the eastern Pyrenees. *Catena*
762 *Suppl.* **13:** 79-95.
763 Gallart F, Llorens P, Latron J, Regüés D. 2002. Hydrological processes and their seasonal
764 controls in a small Mediterranean mountain catchment in the Pyrenees. *Hydrology and*
765 *Earth System Sciences* **6:** 527-537. DOI:10.5194/hess-6-527-2002.
766 Gallart F, Pérez-Gallego N, Latron J, Martínez-Carreras N, Nord G. 2013. Short- and
767 long-term studies of sediment dynamics in a small humid Mediterranean basin with
768 badlands. *Geomorphology* **196:** 242-251. DOI:10.1016/j.geomorph.2012.05.028.
769 García-Orellana, J, Sánchez-Cabrera JA, Masqué P, Àvila A, Costa E, Loÿe-Pilot MD,
770 Bruach-Menchén JM. 2006. Atmospheric fluxes of ^{210}Pb to the western Mediterranean

771 Sea and the Saharan dust influence. *Journal of Geophysical Research* **111:** D15305.
772 DOI:10.1029/2005JD006660.
773 García-Ruiz JM, Nadal-Romero E, Lana-Renault N, Beguería S. 2013. Erosion in
774 Mediterranean landscapes: Changes and future challenges. *Geomorphology* **198:** 20-
775 36. DOI:10.1016/j.geomorph.2013.05.023.
776 García-Ruiz JM, Beguería S, Lana-Renault N, Nadal-Romero E, Cerdà A. 2017. Ongoing
777 and emerging questions in water erosion studies. *Land Degradation and Development*
778 **28:** 5-21. DOI:10.1002/ldr.2641.
779 Hancock GJ, Wilkinson SN, Hawdon AA, Keen RJ. 2014. Use of fallout tracers ^{7}Be,
780 ^{210}Pb and ^{137}Cs to distinguish the form of sub-surface soil erosion delivering sediment
781 to rivers in large catchments. *Hydrological Processes* **28:** 3855-3874.
782 DOI:10.1002/hyp.9926.
783 He Q, Walling DE. 1996. Interpreting particle size effects in the adsorption of ^{137}Cs and
784 unsupported ^{210}Pb by mineral soils and sediments. *Journal of Environmental*
785 *Radioactivity* **30:** 117-137. DOI:10.1016/0265-931X(96)89275-7.
786 Latron J, Llorens P, Gallart F. 2009. The hydrology of Mediterranean mountain areas.
787 *Geography Compass* **3:** 2045-2064. DOI:10.1111/j.1749-8198.2009.00287.x.
788 Lexartza-Artza I, Wainwright J. 2011. Making connections: changing sediment sources
789 and sinks in an upland catchment. *Earth Surface Processes and Landforms* **36:** 1090-
790 1104. DOI:10.1002/esp.2134.
791 Llorens P., Queralt I, Plana F, Gallart F. 1997. Studying solute and particulate sediment
792 transfer in a small Mediterranean mountainous catchment subject to land
793 abandonment. *Earth Surface Processes and Landforms* **22:** 1027-1035.
794 DOI:10.1002/(SICI)1096-9837(199711)22:11<1027::AID-ESP799>3.0.CO;2-1.

López-Tarazón JA, Batalla RJ, Vericat D. 2011. In-channel sediment storage in a highly erodible catchment: the River Isábena (Ebro Basin, southern Pyrenees). *Zeitschrift für Geomorphologie* **55:** 365-382. DOI:10.1127/0372-8854/2011/0045.

López-Tarazón JA, Batalla RJ, Vericat D, Francke T. 2012. The sediment budget of a highly dynamic mesoscale catchment: The River Isábena. *Geomorphology* **138:** 15-28. DOI:10.1016/j.geomorph.2011.08.020.

Mabit L, Benmansour M, Walling DE. 2008. Comparative advantages and limitations of the fallout radionuclides ^{137}Cs, $^{210}Pb_{ex}$ and ^{7}Be for assessing soil erosion and sedimentation. *Journal of Environmental Radioactivity* **99:** 1799-1807. DOI:10.1016/j.jenvrad.2008.08.009.

Mabit L, Klik A, Toloza A. 2010. Radioisotopic measurements (^{137}Cs and ^{210}Pb) to assess erosion and sedimentation processes: case study in Austria. In *Land Degradation and Desertification: Assessment, Mitigation and Remediation*, Zdruli P, Pagliai M, Kapur S, Faz-Cano A (eds). Springer: Dordretch; 401-412.

Mabit L, Benmansour M, Abril JM, Walling DE, Meusburger K, Iurian AR, Bernard C, Tarján S, Owens PN, Blake WH, Alewell C. 2014. Fallout ^{210}Pb as a soil and sediment tracer in catchment sediment budget investigations: A review. *Earth-Science Reviews* **138:** 335-351. DOI:10.1016/j.earscirev.2014.06.007.

Mano V, Némery J. Belleudy P, Poirel A. 2009. Assessment of suspended sediment transport in four Alpine watersheds (France): influence of the climatic regime. *Hydrological Processes* **23:** 777-792. DOI:10.1002/hyp.7178.

Martínez-Carreras N, Soler M, Hernández E, Gallart F. 2007. Simulating badlands erosion with KINEROS2 in a small Mediterranean mountain basin (Vallcebre, Eastern Pyrenees). *Catena* **71:** 145-154. DOI:10.1016/j.catena.2006.05.013.

819 Moreno-de las Heras M, Gallart F. 2016. Lithology controls the regional distribution and
820 morphological diversity of montane Mediterranean badlands in the upper Llobregat
821 basin (eastern Pyrenees). *Geomorphology* **273:** 107-115.
822 DOI:10.1016/j.geomorph.2016.08.004.
823 Mathys N, Brochot S, Meunier M, Richard D. 2003. Erosion quantification in the small
824 marly experimental catchments of Draix (Alpes de Haute Provence, France).
825 Calibration of the ETC rainfall-runoff-erosion model. *Catena* **50:** 527-548.
826 DOI:10.1016/S0341-8162(02)00122-4.
827 Nadal-Romero E, Latron J, Martí-Bono C, Regüés D. 2008. Temporal distribution of
828 suspended sediment transport in a humid Mediterranean badland area: the Araguás
829 catchment, Central Pyrenees. *Geomorphology* **97:** 601-616.
830 DOI:10.1016/j.geomorph.2007.09.009.
831 Nadal-Romero E, Martínez-Murillo JF, Vanmaercke M, Poesen J. 2011. Scale-
832 dependency of sediment yield from badland areas in Mediterranean environments.
833 *Progress in Physical Geography* **35:** 297-332. DOI:10.1177/0309133311400330.
834 Nord G, Soler M, Latron J, Gallart F. 2010. Observations on flow hydraulics in a gauging
835 station of a small stream with high suspended sediment load (Vallcebre, eastern
836 Pyrenees). In *Sediment Dynamics for a Changing Future*, IAHS Publ. **337**, Banasik K,
837 Horowitz AJ, Owens PN, Stone M, Walling DE (eds). IAHS Press: Wallingford; 238-
838 244.
839 Olley J, Caitcheon G. 2000. Major element chemistry of sediments from the darling-
840 Barwon river and its tributaries: implications for sediment and phosphorous sources.
841 *Hydrological Processes*, **14:** 1159-1175. DOI:10.1002/(SICI)1099-
842 1085(200005)14:7<1159::AID-HYP6>3.0.CO;2-P.

Phillips JM, Russel MA, Walling DE. 2000. Time-integrated sampling of fluvial suspended sediment: a simple methodology for small catchments. *Hydrological Processes* **14:** 2589-2602. DOI:10.1002/1099-1085(20001015)14:14<2589::AID-HYP94>3.0.CO;2-D.

Piqué G, López-Tarazón JA, Batalla RJ. 2014. Variability of in-channel sediment storage in a river draining highly erodible areas (the Isábena, Ebro Basin). *Journal of Soil and Sediments* **14:** 2031-2044. DOI:10.1007/s11368-014-0957-6.

Porto P, Walling DE, Tamburino V, Callegari G. 2003. Relating caesium-137 and soil loss for cultivated land. *Catena* **53:** 303-326. DOI:10.1016/S0341-8162(03)00084-5.

Porto P, Walling DE, Callegari G. 2013. Using ^{137}Cs and $^{210}Pb_{ex}$ measurements to investigate the sediment budget of a small forested catchment in southern Italy. *Hydrological Processes* **27:** 795-806. DOI:10.1002/hyp.9471.

Poyatos R, Latron J, Llorens P. 2003. Land use and land cover change after agricultural abandonment – the case of a Mediterranean mountain area (Catalan Pre-Pyrenees). *Mountain Research and Development* **23:** 362-368. DOI:10.1659/0276-4741(2003)023[0362:LUALCC]2.0.CO;2.

Regüés D, Gallart F. 2004. Seasonal patterns of runoff and erosion responses to simulated rainfall in a badland area in Mediterranean mountain conditions (Vallcebre, southeastern Pyrenees). *Earth Surface Processes and Landforms* **29:** 755-767. DOI:10.1002/esp.1067.

Regüés D, Pardini G, Gallart F. 1995. Regolith behavior and physical weathering of clayey mudrock as dependent on seasonal weather conditions in a badland area at Vallcebre, Eastern Pyrenees. *Catena* **25:** 199-212. DOI:10.1016/0341-8162(95)00010-P.

867 Regüés D, Nadal-Romero E. 2012. Uncertainty in the evaluation of sediment yield from
868 badland areas: Suspended sediment transport estimated in the Araguás catchment
869 (central Spanish Pyrenees). *Catena* **106:** 93-100. DOI:10.1016/j.catena.2012.05.006.
870 Serrano-Muela MP, Nadal-Romero E, Lana-Renault N, González-Hidalgo JC, López-
871 Moreno JI, Beguería S, Sanjuan Y, García-Ruiz JM. 2015. An exceptional rainfall
872 event in the central western Pyrenees: spatial patterns in discharge and impact. *Land*
873 *Degradation and Development* **26:** 249-262. DOI:10.1002/ldr.2221.
874 Smith HG, Blake WH. 2014. Sediment fingerprinting in agricultural catchments: A
875 critical re-examination of source discrimination and data corrections. *Geomorphology*
876 **204:** 177-191. DOI:10.1016/j.geomorph.2013.08.003.
877 Solé A, Josa R, Pardini G, Aringhieri R, Plana F, Gallart F. 1992. How mudrock and soil
878 physical properties influence badland formation at Vallcebre (Pre-Pyrenees, NE
879 Spain). *Catena* **19:** 287-300. DOI:10.1016/0341-8162(92)90003-T.
880 Soler M, Regüés D, Gallart F. 2006. Automatic sampler calibration to estimate the
881 collection capacity of suspended sediment. In *Uncertainties in the "Monitoring-*
882 *Conceptualization-Modelling" Sequence of Catchment Research*, Pfister L, Matgen P,
883 van den Bos R, Hoffman L (eds). Centre de Reserche Public Gabriel Lippman:
884 Luxembourg; 425-432.
885 Soler M, Regüés D, Latron J, Gallart F. 2008. Relationships between suspended sediment
886 concentrations and discharge in two small research basins in a mountain
887 Mediterranean area (Vallcebre, Eastern Spain). *Geomorphology* **98:** 143-152. DOI:
888 10.1016/j.geomorph.2007.02.032.
889 Soler M, Nord G, Catari G, Gallart F. 2012. Assessment of suspended sediment
890 concentration measurement error in relation to particle size, using continuous sensors

891 in a small mountain stream (Vallcebre catchments, Eastern Pyrenees). *Zeitschrift für*
892 *Geomorphologie, Suppl. Vol.* **56:** 99-113. DOI:10.1127/0372-8854/2012/S-00106.
893 Vanmaercke M, Poesen J, Verstraeten G., de Vente J, Ocakoglu F. 2011. Sediment yield
894 in Europe: spatial patterns and scale dependency. *Geomorphology* **130:** 142-161.
895 DOI:10.1016/j.geomorph.2011.03.010.
896 Wainwright J, Thornes JB. 2004. *Environmental Issues in the Mediterranean: Processes*
897 *and Perspectives from the Past and Present*. Routledge: London.
898 Wainwright J, Turnbull L, Ibrahim TG, Lexartza-Artza I, Thornton SF, Brazier R. 2011.
899 Linking environmental regimes, space and time: interpretations of structural and
900 functional connectivity. *Geomorphology* **126:** 387-404.
901 DOI:10.1016/j.geomorph.2010.07.027.
902 Wallbrink P, Olley JM, Hancock G. 2002. Estimating residence times of fine sediment in
903 river channels using fallout ^{210}Pb. In *The Structure, Function and Management*
904 *Implications of Fluvial Sedimentary Systems*, IAHS Publ. **276**, Dyer FJ, Thoms MC,
905 Olley JM (eds). IAHS Press: Wallingford; 425-432.
906 Walling DE. 1983. The sediment delivery problem. *Journal of Hydrology* **65:** 209-237.
907 DOI:10.1016/0022-1694(83)90217-2.
908 Walling DE. 2003. Using environmental radionuclides as tracers in sediment budget
909 investigations. In *Erosion and Sediment Transport Measurement in Rivers:*
910 *Technological and Methodological Advances*, IAHS Publ. **283**, Bogen J, Fergus T,
911 Walling DE (eds). IAHS Press: Wallingford; 57-78.
912 Walling DE. 2005. Tracing suspended sediment sources in catchments and river systems.
913 *Science of the Total Environment* **334:** 159-184.
914 DOI:10.1016/j.scitotenv.2005.02.011.

915 Walling DE, Schuller P, Zhang Y, Iroume A. 2009. Extending the timescale for using
916 beryllium 7 measurements to document soil redistribution by erosion. *Water*
917 *Resources Research* **45:** W02418. DOI:10.1029/2008WR007143.
918 Wethered AS, Ralph TJ, Smith HG, Fryirs KA, Heijnis H. 2015. Quantifying fluvial
919 (dis)connectivity in an agricultural catchment using a geomorphic approach and
920 sediment source tracing. *Journal of Soils and Sediments* **15:** 2052-2066.
921 DOI:10.1007/s11368-015-1202-7.
922 Wilkinson SN, Olley JM, Furuichi T, Burton J, Kinsey-Henderson AE. 2015. Sediment
923 source tracing with stratified sampling and weightings based on spatial gradients in
924 soil erosion. *Journal of Soils and Sediments* **15:** 2038-2051. DOI:10.1007/s11368-
925 015-1134-2.

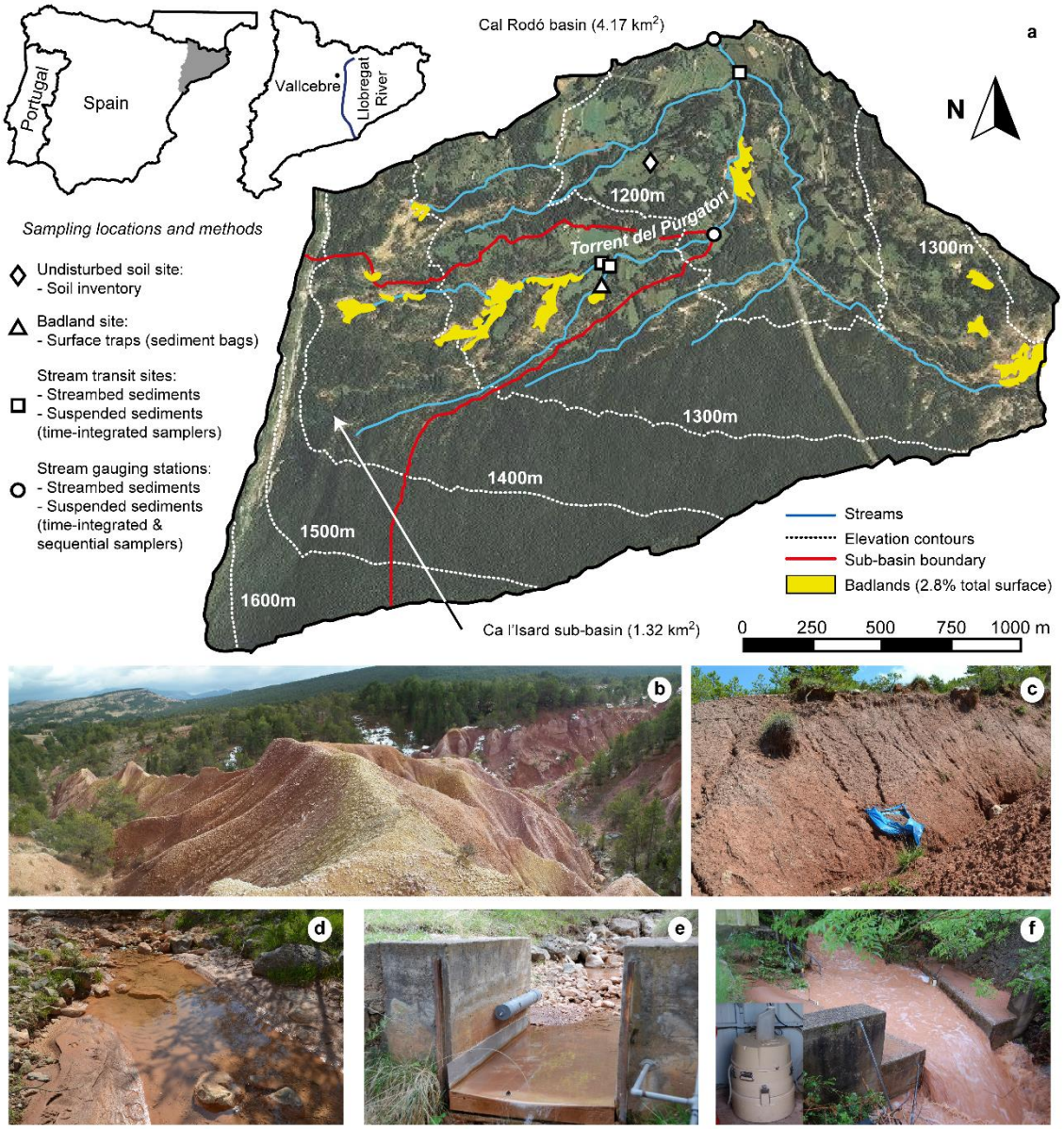

Figure 1. Location map and experimental setup: (a) map of the Vallcebre research catchments (Cal Rodó basin and Ca l'Isard sub-basin) with details of the sediment sampling locations; (b) general view of a badland within Ca l'Isard sub-basin; (c) surface trap of sediments (permeable bag) at a badland surface; (d) streambed sediment deposit in Torrent del Purgatori; (e) Ca l'Isard gauging station with detail of a time-integrated sediment sampler on the wall; (f) runoff flow event at Cal Rodó gauging station (with detail of an *ISCO* sequential sediment sampler). Source for background image: Institut Cartogràfic i Geològic de Catalunya (a). Pictures by M. Moreno-de las Heras (b), F. Gallart (c-d) and J. Latron (e-f).

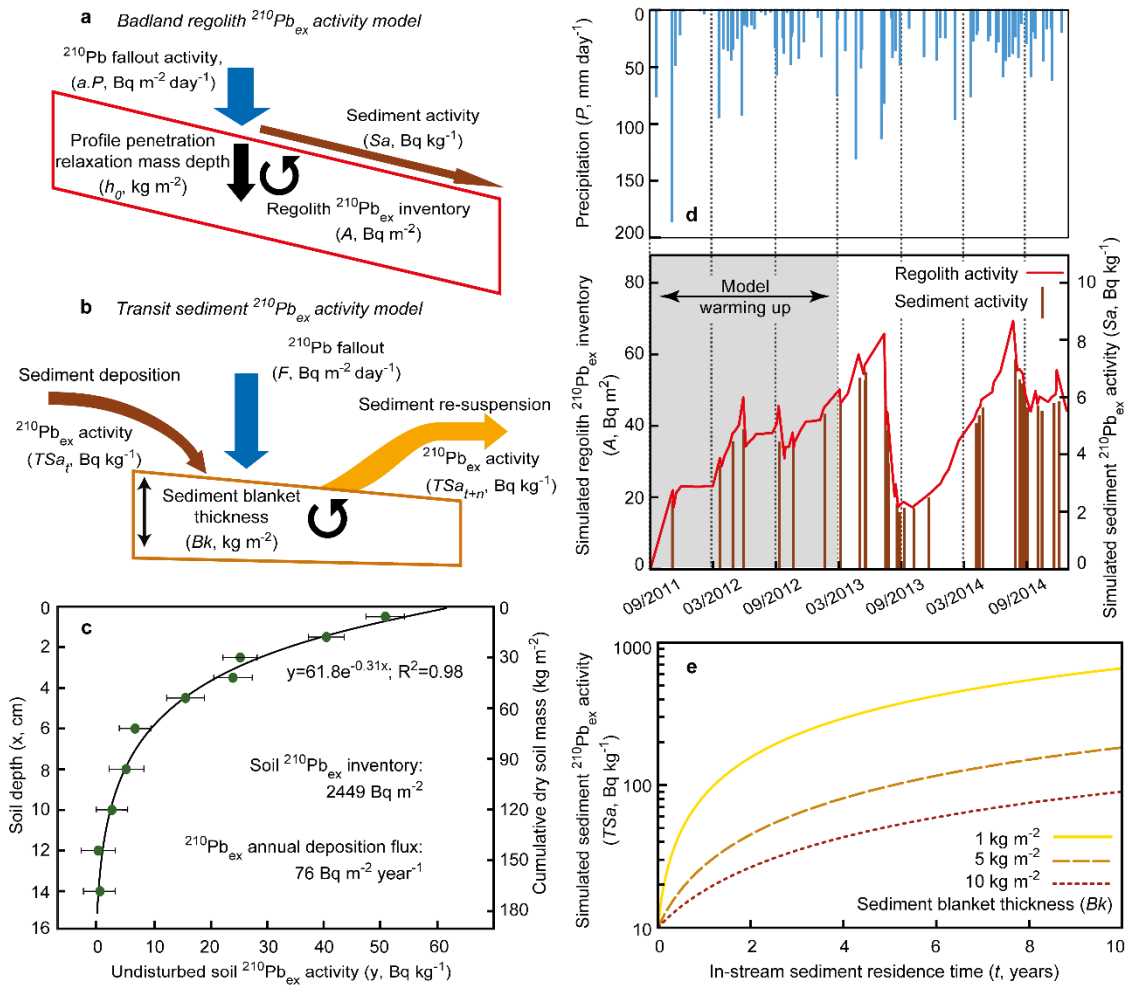

Figure 2. $^{210}Pb_{ex}$ modelling details: diagrams of (a) the badland regolith and (b) transit sediment $^{210}Pb_{ex}$ activity models; (c) the reference, undisturbed soil $^{210}Pb_{ex}$ inventory used for parameterizing the fallout 210-lead atmospheric flux in the mass-balance models (soil profile 40 x 40 cm surface, 15 cm depth; sampling site location is shown in Figure 1a); (d) simulated $^{210}Pb_{ex}$ at the badland surfaces (daily time step); (e) simulated effect of in-stream sediment residence time on sediment $^{210}Pb_{ex}$ activity. Bars in panel (c) indicate the analytical error.

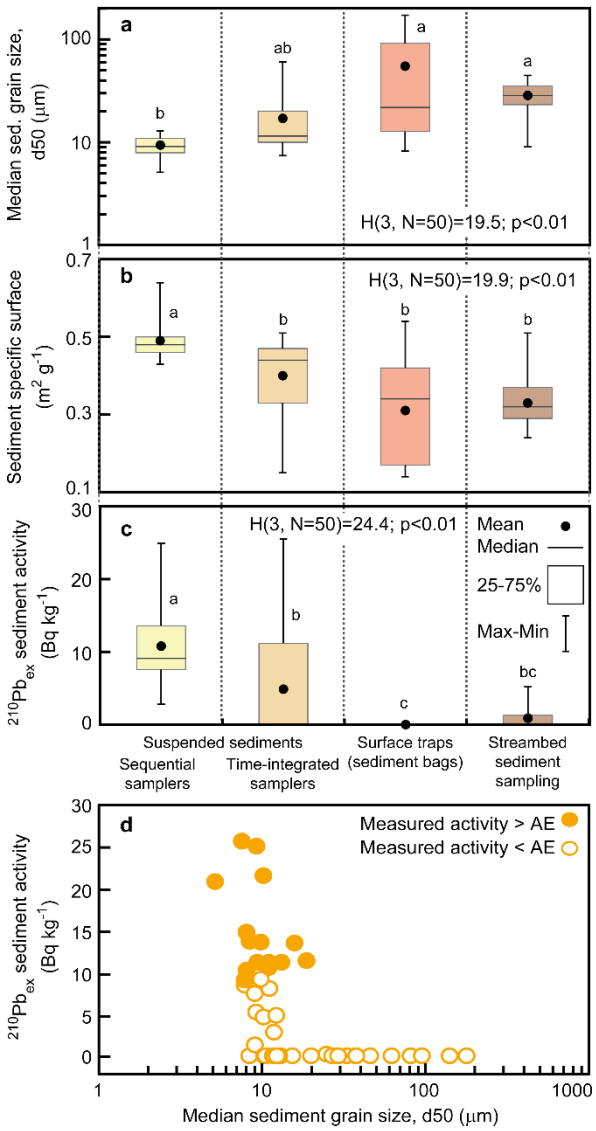

945

946 Figure 3. Effect of sediment sampling method on (a) median (d50) sediment grain size,
947 (b) specific surface area of sediment, and (c) $^{210}Pb_{ex}$ sediment activity. Graph (d)
948 illustrates the general influence of sediment grain size on $^{210}Pb_{ex}$ sediment activity
949 (black/grey circles indicate $^{210}Pb_{ex}$ data with analytical error below/above 100% of
950 measured value). Abbreviations: AE, analytical error.

951

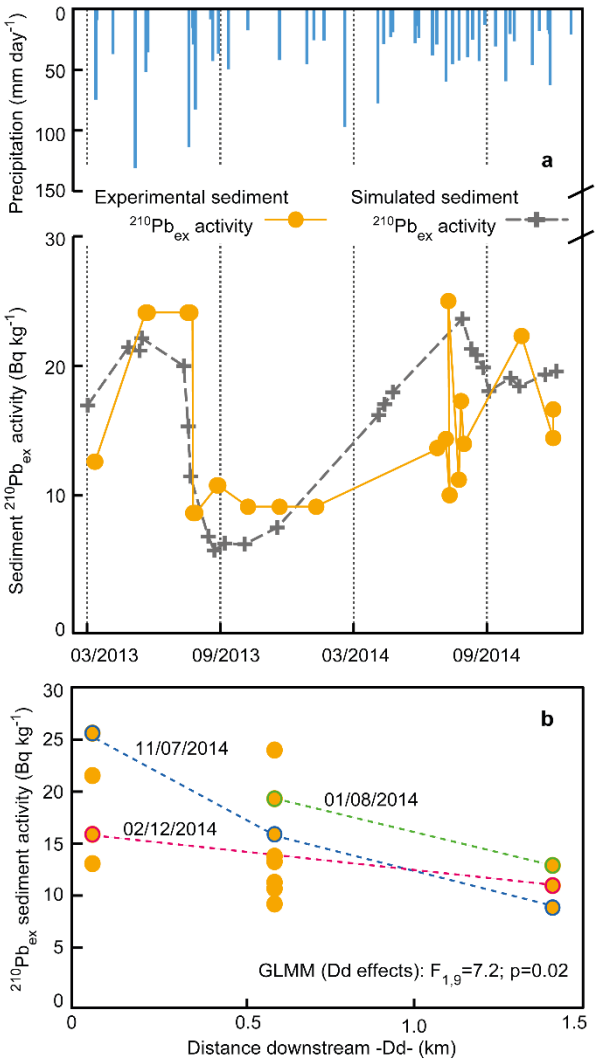

Figure 4. Spatiotemporal patterns of sediment $^{210}Pb_{ex}$ activities: (a) temporal pattern of daily precipitation, as well as simulated and experimentally measured sediment $^{210}Pb_{ex}$ activities; (b) influence of downstream distance on measured sediment $^{210}Pb_{ex}$ activity (the dotted lines connect the samples for three flow events with available paired measurements for the sampling locations). Abbreviations: GLMM, general linear mixed model statistics. Notes: spatiotemporal data were analysed by the experimental sediment $^{210}Pb_{ex}$ records with analytical error below 100% of measured values; simulated sediment $^{210}Pb_{ex}$ activities in graph (a) were particle-size corrected by use of eq. 8 along with the mean specific surface area (SSA) of displayed experimental sediments (0.50 m^2 g^{-1}) and the SSA estimate for the badland regoliths (0.14 m^2 g^{-1}).